科学通报 2025 年 第 70 卷 第 14 期: 2163 ~ 2175

《中国科学》杂志社
SCIENCE CHINA PRESS

评 述

俯冲带板片混杂岩底辟作用

刘汇川[1,2], 王岳军[3*], 皇甫鹏鹏[4*]

1. 中国石油大学(北京)油气资源与工程全国重点实验室, 北京 102249
2. 中国石油大学(北京)地球科学学院, 北京 102249
3. 中山大学地球科学与工程学院, 广东省地球动力作用与地质灾害重点实验室, 珠海 519080
4. 中国科学院大学地球与行星科学学院, 地球系统数值模拟与应用全国重点实验室, 北京 101408
* 联系人, E-mail: wangyuejun@mail.sysu.edu.cn; huangfu@ucas.ac.cn

2025-01-03 收稿, 2025-03-06 修回, 2025-04-12 接受, 2025-04-17 网络版发表
国家自然科学基金(42472181, 42030307)和国家重点研发计划(2021YFA071900, 2022YFF0800704)资助

摘要 俯冲大洋板片与地幔如何相互作用及形成弧岩浆岩的过程, 是当今地球科学的关键科学问题. 传统观点认为俯冲板片流体和熔体交代的地幔楔部分熔融形成弧岩浆岩. 近年学者提出板片混杂岩底辟体与弧下地幔物理混合后再部分熔融也可形成弧岩浆岩. 但板片混杂岩底辟体与地幔如何相互作用、相互作用形成何种产物、如何有效识别这些产物, 是大地构造学亟待解决的科学问题. 本文综述了近年有关板片混杂岩底辟作用的研究资料, 列举了板片混杂岩底辟体与弧下地幔物理混合形成弧岩浆岩的相关证据, 并依据数值模拟将板片混杂岩底辟体细分为大洋沉积物底辟、混杂岩底辟和蚀变洋壳底辟等三个过程. 综述发现全岩Sr-Nd-Hf-O等同位素组成及其比值的联合使用可区分板片流体/熔体交代和混杂岩底辟物理混合两种模式. 俯冲大洋沉积物底辟体具低δ^{30}Si和$\delta^{138/134}$Ba值、高$\varepsilon_{\mathrm{Hf}}(t)$和$\delta^{18}$O值、全岩Nd-Hf同位素解耦等特征, 而蚀变洋壳底辟体具有重的Mg、B和Ba同位素及轻的O和Li同位素. 板片混杂岩与弧下地幔或OIB(洋岛玄武岩)型地幔混合可形成铌钽亏损弧岩浆岩或富铌弧岩浆岩. 板片混杂岩底辟的研究仍存在一些问题静待地质学家深入研究.

关键词 板片混杂岩, 底辟, 蚀变洋壳, 弧下地幔, 弧岩浆岩

俯冲大洋板片混杂岩由地幔橄榄岩、蚀变洋壳和大洋沉积物组成, 其在汇聚板块边缘与弧下地幔如何相互作用及形成弧岩浆岩的过程, 是当今大地构造学的关键热点科学问题. 传统观点认为俯冲大洋板片流体和熔体交代的地幔楔部分熔融形成了亏损高场强元素的弧岩浆岩(图1(a)), 已被地质学家视之为经典[1~6]. 实验岩石学研究表明, 在俯冲带高压(2.7~5 GPa)背景下只有当温度高于1050°C时, 大洋沉积物部分熔融体才表现出弧型的特征, 但俯冲大洋板片与弧下地幔的界面处常难以达到如此高温. 同时, 数值模拟[7~9]、地震观测[10]和地球化学储库的完善[1,11~14]等已然对这一传统弧岩浆岩形成过程发起了挑战或质疑. 基于此, 地质学家提出了另一种俯冲板片与弧下地幔相互作用的模型, 即蚀变洋壳和大洋沉积物形成的板片混杂岩底辟体与弧下地幔物理混合后部分熔融形成弧岩浆岩(图1(b))[10~12,14~20]. 两种模型的差异性在于: (1) 前者是化学交代反应, 后者是物理混合; (2) 前者是板片脱水/部分熔融产物交代的地幔楔部分熔融, 后者是板片混杂岩与地幔楔物理混合后的部分熔融[12,14,18].

板片混杂岩底辟体(mélange diapir)在一些文献中也被称为地幔楔柱(mantle wedge plume)或者冷柱(cold plume)[8,9,21~25]. 为了不与地幔柱(mantle plume)的概念混淆, 本文统一称之为板片混杂岩底辟体. 混杂岩底辟

引用格式: 刘汇川, 王岳军, 皇甫鹏鹏. 俯冲带板片混杂岩底辟作用. 科学通报, 2025, 70: 2163–2175
Liu H, Wang Y, Huangfu P. Mélange diapirs in the subduction factory (in Chinese). Chin Sci Bull, 2025, 70: 2163–2175, doi: 10.1360/TB-2025-0017

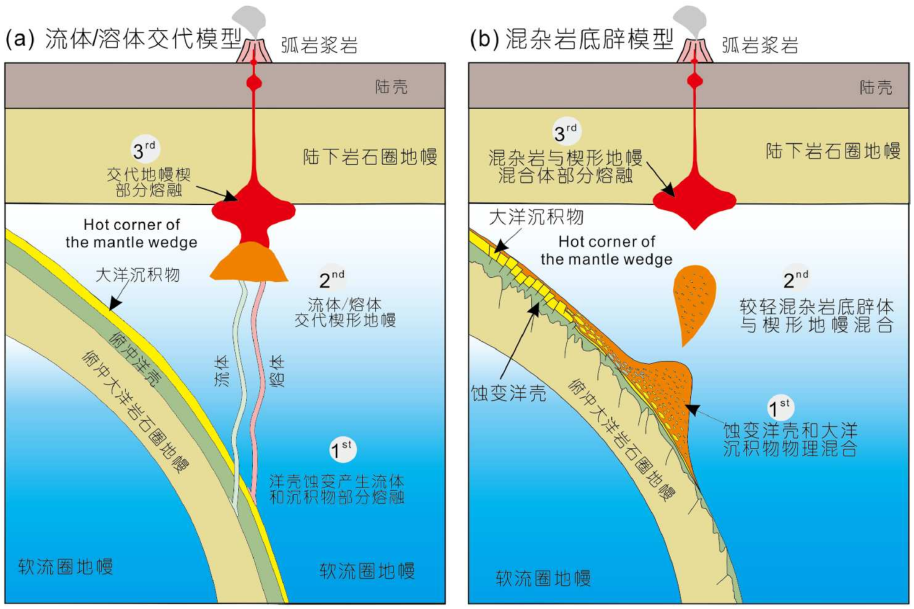

图 1 俯冲板片与弧下地幔相互作用形成弧岩浆岩的两种模型[13,14]. (a) 板片流体/沉积物熔体交代楔形地幔形成弧岩浆岩的传统模型; (b) 板片混杂岩底辟体与楔形地幔物理混合再部分熔融形成弧岩浆岩的新模型

Figure 1 Illustration of two different end-member models of slab material transport in subduction zones[13,14]. (a) In the conventional model, sediment melts and fluids from altered oceanic crust (AOC) mix with ambient mantle melts to form arc magmas. (b) In the mélange model, sediments, AOC, and hydrated mantle physically mix to form hybrid mélange rocks

体由蚀变洋壳和大洋沉积物碎块组成[14], 起源于俯冲大洋板片与楔形地幔的界面处, 底辟进入楔形地幔后与楔形地幔物理混合(图1(b)), 最后减压熔融形成弧岩浆岩. 尽管俯冲板片混杂岩底辟模型被越来越多的研究者所关注, 但对其认识仍处于不断完善之中[10,12,14,15,17~20]. 对证实板片混杂岩底辟体存在的证据、板片混杂岩的底劈方式、如何与地幔相互作用, 所形成的岩浆产物具怎样的特征、如何有效识别等, 仍是大地构造学亟待解决的前沿科学问题. 本文结合作者近年发表有关板片混杂岩底辟体的多篇文章, 详细综述了当前对俯冲板片混杂岩底辟作用的研究现状.

1 俯冲板片混杂岩底辟体存在的证据

底辟的概念最早指在构造应力的作用下, 或者由于岩石物质间密度倒置所引起的浮力作用, 高塑性岩石(如盐、石膏、黏土、页岩及煤层等)向上推挤或刺穿而挤入上覆岩层[26,27]. 俯冲板片混杂岩底辟的概念, 最早出现于Becker和Cloos(1985)的描述[28]. 早期学者认为俯冲板片混杂岩底辟发生在俯冲带上盘上地壳浅部[28~34], 后来数值模拟工作发现俯冲板片混杂岩底辟也可发生在70 km, 甚至100 km以上深度[9,35]. 现有如下证据也证明板片混杂岩在俯冲过程中能发生底辟.

1.1 地球物理和数值模拟的证据

俯冲板片混杂岩底辟模型以前之所以未被重视, 主要是因为前人在地震成像观测研究中没有从正在发育的俯冲带地幔楔中识别出底辟的板片混杂岩[36~38]. 近年, 在台湾北部的菲律宾洋板块向欧亚大陆下俯冲形成的楔形地幔中, Lin等人[10]识别出地震散射障碍体, 其深度介于弧下60~95 km, 被认为是板片混杂岩底辟体存在的直接证据. Zheng等人[36]在南太平洋汤加地幔楔内识别出与大量交代反应伴生近水平地震波反射界面, 但界面深度过深, 能否代表底辟的板片混杂岩仍不确定. 但必须看到的是: 板片混杂岩底辟体之所以难以通过地震成像观测到, 既与单个板片混杂岩底辟体体积小且与地幔楔边界不甚明显有关, 也与板片混杂岩底辟体与地幔楔物理混合后可能迅速部分熔融在地幔楔中残留时间过短有关[10].

Hall和Kincaid[35]的物理模拟实验证实俯冲板片混杂岩可形成底辟体, 并发现板片混杂岩底辟体与地幔流相互作用形成低密度低黏度的管状流体. 随后, 前人

开展了大量数值模拟工作以探索板片混杂岩底辟体存在的理论基础和前提条件[7~9,20,23~25,39~42]. Gerya和Yuen[9]模拟发现瑞利-泰勒不稳定可导致俯冲板片上部形成明显不同于热的板片流体/熔体的冷柱(cold plume), 该冷柱比软流圈低300~400°C, 起源深度可能超过100 km. 对该冷柱物理结构的进一步热力学模拟发现, 冷柱靠近板片的底部地震正异常, 冷柱头部地震负异常[8], 这为Lin等人[10]在台湾北部弧下地幔发现地震散射障碍体提供了灵感. Gorczyk等人[25]以数值模拟对日本Horoman超基性杂岩体的解剖分析, 在楔形地幔柱内识别出了大洋岩石圈地幔橄榄岩、俯冲洋壳和固态地幔等端元. Currie等人[41]开展的俯冲板片混杂岩中大洋沉积物底辟过程模拟, 显示因其密度远小于地幔, 当厚度大于350 m时, 大洋沉积物底辟作用在100 km深度就很显著. 而Behn等人[20]通过计算得到, 即便很薄的大洋沉积物也可形成底辟体, 且底辟作用从40 km深度即已开始. Miller和Behn[42]模拟认为俯冲到80 km左右, 大洋沉积物底辟体会快速形成, 在温度超过900°C时大洋沉积物在1~3 Ma内就会脱离板片, 向上底辟. Zhang等人[39]的数值模拟表明当大洋沉积层厚度在0.2~1.1 km时, 大洋沉积物底辟体半径介于0.7~3.7 km间, 且底辟深度越浅底辟体半径越大, 当底辟深度为25 km底辟体半径可达2.4~3.7 km. 其底辟过程主要受控于大洋沉积物厚度、大洋沉积物矿物组成和俯冲板片的热状态[40]. 尽管前人开展的模拟研究主要针对板片混杂岩中最上部的大洋沉积物, 但这些模拟结果为我们认识俯冲带内板片混杂岩是否可底辟提供了理论依据.

1.2 岩石学和地球化学证据

Cruz-Uribe等人[15]和Codillo等人[11]的Piston-Cylinder实验确定不同比例板片混杂岩和弧下地幔物理混合后部分熔融可形成拉斑质、钙碱性和碱性的弧岩浆岩. 受俯冲板片改造前的弧下地幔和蚀变洋壳均具有较低的高场强元素和大离子亲石元素含量. 弧下地幔和俯冲板片中副矿物(比如, 金红石、榍石和钙钛矿)选择性地富集高场强元素, 可很好解释弧岩浆岩亏损高场强元素的特征(如Nb-Ta-Ti负异常)[12,43]. 大洋沉积物富集大离子亲石元素和稀土元素, 其少量混入即可显著改变地幔楔的微量元素组成[11].

大洋沉积物熔体和蚀变洋壳流体与大洋沉积物和蚀变洋壳分别具有相同的Sr-Nd同位素组成和较低Nd/Sr比值. 因此, 流体/熔体交代地幔和板片混杂岩(大洋沉积物和蚀变洋壳)与地幔物理混合的Sr-Nd同位素两端元混合曲线, 具有不同的曲率. Nielsen和Marschall[14]依据这一特征构建了区分流体/熔体交代地幔和板片混杂岩与地幔物理混合两种情形的微量元素和Sr-Nd同位素组分联用方法. 随后众多学者以此为依据在全球不同位置弧下地幔楔中识别出了板片混杂岩底辟体[13,17,44~46]. 而近年稳定同位素储库不断完善, 如Ba、B、Mg, O、Mo和Si等同位素体系, 均被成功用于示踪俯冲带弧岩浆岩源区中是否有蚀变洋壳和大洋沉积物底辟体参与[1,13,17,45~47].

2 基于数值模拟重建的俯冲板片混杂岩底辟过程

2.1 初始模型的建立

物理和数值模拟是探索俯冲板片混杂岩底辟过程的有效手段. 现有的研究多针对与弧下地幔密度差较大的大洋沉积物底辟过程[7~9,20,23~25,35,39~42], 对混杂岩整体和下部蚀变洋壳的底辟过程研究相对薄弱. 笔者使用算法“I2VIS”[9,48,49]开展二维数值模拟重建了板片混杂岩底辟和蚀变洋壳循环过程[50].

基于“I2VIS”算法设置了4000 km×670 km的初始模型, 代表洋陆俯冲体系(图2). 这一模型包含了非均匀的699×134矩形网格, 其分辨率从俯冲碰撞区的2 km×2 km到模型边界附近的30 km×30 km不等. 模型左侧是2000 km长的大洋岩石圈, 右侧是2000 km长的大陆岩石圈, 两者之间为旨在诱发大洋俯冲的薄弱带. 大洋和大陆岩石圈分别设置为76和120 km厚, 洋壳、大陆上地壳和大陆下地壳的初始厚度分别为8、20和15 km. 沉积物和大陆上地壳用含水石英岩流变代表, 洋壳和大陆下地壳用斜长石代表. 岩石圈地幔和软流层均用干橄榄石代表. 以1 cm/a(图3)和3 cm/a(图4)两个汇聚速度开展模拟, 其中1 cm/a的模拟考虑了洋壳在高温高压下相变带来的密度变化的影响. 数值方法和模型配置的详细信息可以参考Liu等人[50].

2.2 数值模拟结果

模拟结果显示低速(1 cm/a)俯冲过程中, 板片混杂岩在较浅的深度(<80 km)就开始底辟(图3). 因底辟深度浅和底辟速率快, 大洋沉积物和蚀变洋壳底辟几乎同时发生, 难以区分. 而在较高的俯冲速率下(3 cm/a),

持续俯冲的大洋板片混杂岩会经历三阶段底辟(图4): (1) 大洋沉积物底辟; (2) 混杂岩(大洋沉积物和蚀变洋壳混合)底辟; (3) 蚀变洋壳底辟. 大洋沉积物在俯冲带各端元中密度最小, 无论是热的还是冷的板片高压变

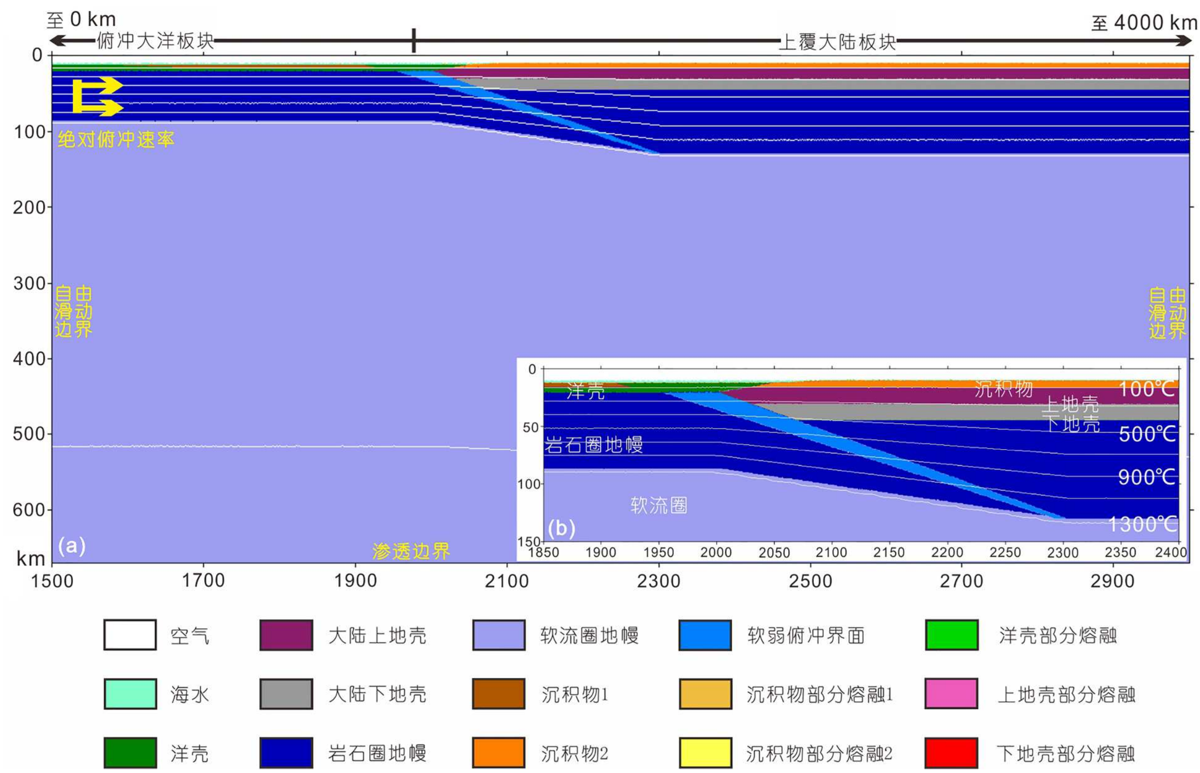

图 2 初始模型. 显示了整体模型(4000 km×670 km)中的大洋俯冲区域(1500 km×500 km). 白线是间隔为200°C的等温线. 该模型左侧为大洋岩石圈, 右侧为大陆岩石圈. 图例中不同的颜色代表不同的岩性. 部分熔融产物的图例将在模型演化过程中出现(图3和4). 不同岩石类型的详细性质见Liu等人[50]

Figure 2 Initial model configurations. Enlargement (1500 km×500 km) of the numerical box (4000 km×670 km) is shown. White lines are isotherms with an interval of 200°C. Two different lithospheres comprise the model, with oceanic on the left and continental on the right. The partially molten crustal rocks will appear during the evolution of the model (Figures 3 and 4). The detailed properties of different rock types can be found in Liu et al. [50]

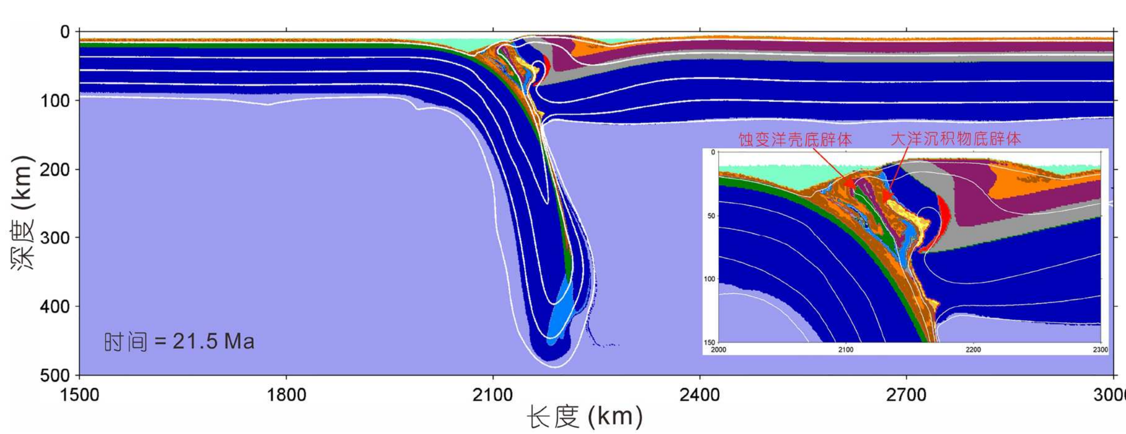

图 3 俯冲板片混杂岩在低速(速度1 cm/a)俯冲汇聚过程中, 底辟过程的数值模拟结果. 白色等温线从100°C开始, 间隔为300°C. 岩石类型的颜色与图2中的颜色相同

Figure 3 Evolution of the numerical model with a convergence velocity of 1 cm/a. Composition evolution is overlapped by white-line isotherms, which are plotted every 300°C starting from 100°C. Colors of rock types are the same as in Figure 2

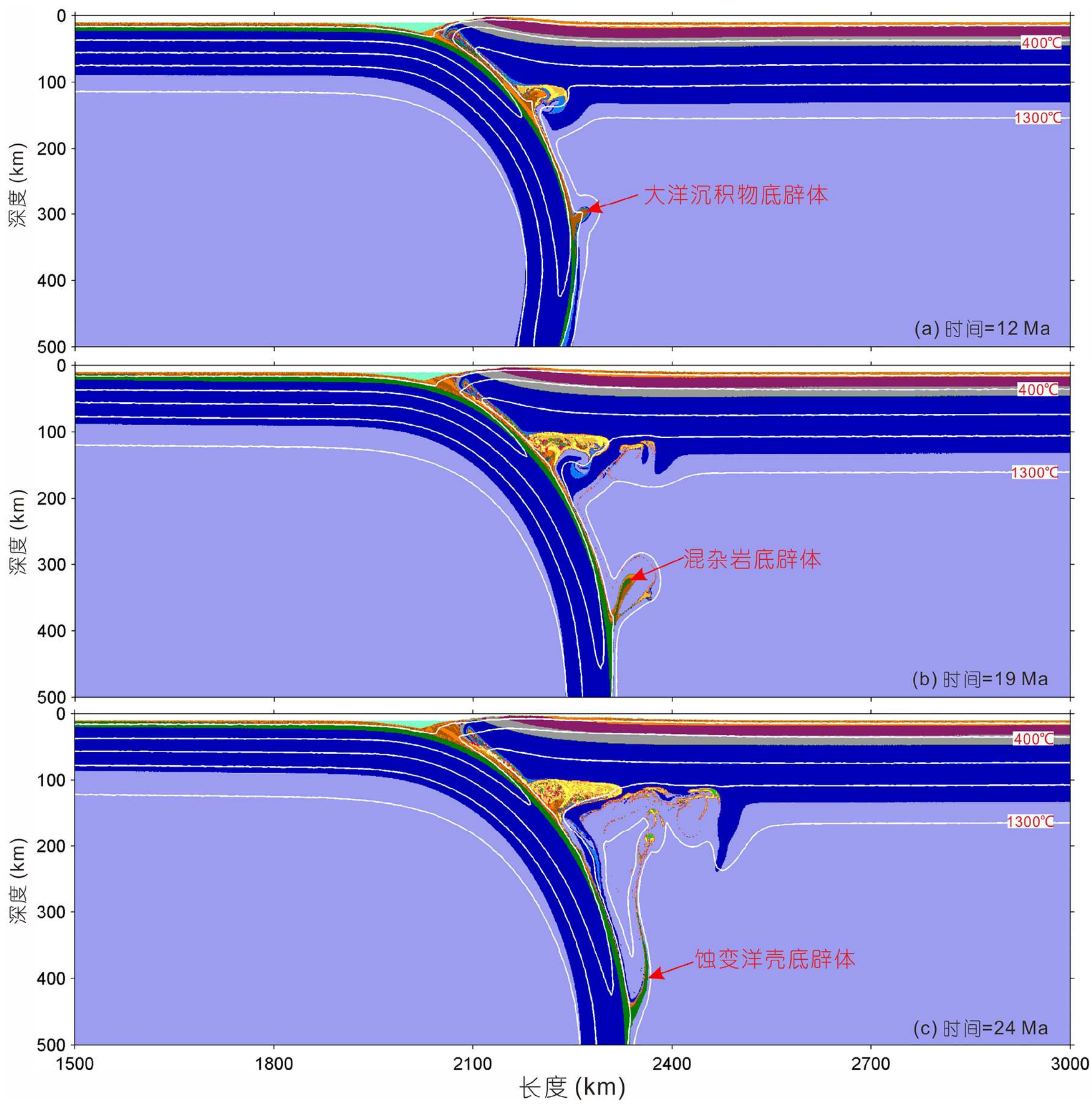

图 4 俯冲板片混杂岩(大洋沉积物和蚀变洋壳)底辟过程的数值模拟结果(速度3 cm/a). 白色等温线从100°C开始, 间隔为300°C. 岩石类型的颜色与图2中的颜色相同. 随着海洋板块的持续俯冲, 大洋沉积物首先底辟(a). 然后, 海洋沉积物和蚀变洋壳的混合物相对于周围的地幔密度较低, 开始底辟(b). 最后, 高温蚀变洋壳较楔形地幔密度低, 也开始底辟(c)

Figure 4 Evolution of the numerical model with a convergence velocity of 3 cm/a. Composition evolution is overlapped by white-line isotherms, which are plotted every 300°C starting from 100°C. Colors of rock types are the same as in Figure 2 With continued subduction of the oceanic plate, the marine sediments upwell firstly from the downgoing slab (a). Then a mixture of the marine sediments and AOC remain buoyant with respect to the surrounding mantle materials, leading to its subsequent upwelling into the overlying mantle wedge (b). At last, such sharp density contrasts between the high-T AOC and mantle wedge after long-term (~24.7 Ma.) subduction of the oceanic plate make the AOC diapir formation and rise up possible (c)

质泥岩与弧下地幔的密度差超过0.3 g/cm^3[20], 因此大部分大洋沉积物在板片俯冲开始阶段即开始上浮脱离板片, 并在上覆岩石圈地幔底部堆积. 洋壳平均密度为3.0 g/cm^3, 高温蚀变的洋壳密度会变小, 明显小于楔形地幔的密度(约3.3 g/cm^3)[8,9,11]. 随着板片持续俯冲(约在24.7 Ma后), 俯冲深度增加, 板片表面部分蚀变洋壳也开始底辟. 在蚀变洋壳和大洋沉积物独立底辟之间, 二者的混合物(即板片混杂岩)底辟. 底辟的混杂岩会经历强烈的部分熔融, 熔融体在岩石圈地幔底部向大陆和大洋两侧扩展延伸, 不断底侵上部岩石圈地幔, 有利于后期底辟的发育. 随着板片的持续俯冲, 三种底辟方式或过程不断重复发生.

3 如何识别弧岩浆源区是否有板片混杂岩参与

如前所述, 地球物理观测、物理数值模拟、实验岩石学和同位素地球化学证据均指示俯冲带板片混杂岩可以底辟, 数值模拟也还原了俯冲板片混杂岩底辟的过程. 如何识别弧岩浆源区是否有板片混杂岩参与则是另一个值得关注的重要科学问题.

3.1 如何区分板片流体/熔体交代和板片混杂岩底辟体物理混合

俯冲板片混杂岩底辟体与楔形地幔混合及流体/熔体交代楔形地幔两种机制形成的弧岩浆岩具相似主量和微量元素组成, 因此传统的元素地球化学特征难以有效辨别弧岩浆岩的上述两种成因, 这限制了我们对俯冲板片与弧下地幔相互作用过程的精细认识. 但是, 两种弧岩浆岩成因机制分别经历的化学交代和物理混合过程能造成多种同位素体系分馏, 这些分馏的同位素体系使我们示踪大洋板片混杂岩在俯冲带与楔形地幔物理混合过程成为可能.

因分配系数差异明显, 俯冲带蚀变洋壳和大洋沉积物在形成流体和熔体过程中微量元素比值(比如Nd/Sr, Hf/Nd等)会发生显著变化. 针对相同同位素体系, 板片流体/熔体交代和板片混杂岩物理混合两种模式表现出完全不同的混合曲线. Nielsen和Marschall[14]建立了一套利用弧岩浆岩全岩Sr-Nd同位素和Sr-Nd-Hf微量元素比值来区分板片流体/熔体交代和板片混杂岩物理混合模式的方法. 比如, (1) 因板片流体/熔体具有较蚀变洋壳和大洋沉积物更低的Nd/Sr元素比值, 板片流体/熔体交代和混杂岩物理混合在Sr-Nd同位素图解上给出了显著差异的混合曲线(图5(a)), 可很好地区分流体/熔体交代和混杂岩物理混合两个过程; (2) 同样因为板片流体/熔体具有较蚀变洋壳和大洋沉积物更低的Nd/Sr元素比值, 混杂岩物理混合的产物在排除了长石分离结晶的情况下, 会落在图5(b)左下角的三角阴影区内, 与板片流体/熔体交代产物完全不同; (3) Hf和Nd两个元素都不是流体活动元素, Hf/Nd比值在地幔部分熔融和岩浆分离结晶过程中保持不变, 但因分配系数的差异混杂岩或者大洋沉积物部分熔融过程中Hf/Nd比值变大(图5(c)). 混杂岩物理混合的产物在图5(c)落在黑色实线上, 再部分熔融因Hf/Nd比值增大会表现出水平延伸的趋势. 图5的三个判别图版已经被广泛用于区分板片流体/熔体交代和板片混杂岩物理混合[13,14,17,19,44~46,50~54].

3.2 如何识别源区是否有大洋沉积物参与

放射性和稳定同位素联合示踪是识别弧岩浆岩源区是否有大洋沉积物参与的有效手段. 比如, 大洋沉积物具有较高的δ^{18}O(最大值超+20 ‰)和亏损的Hf同位素组成($\varepsilon_{Hf}(t)$高达+28), 因此有大洋沉积物参与时弧岩浆岩具有超过地幔的δ^{18}O(+5.6‰)和$\varepsilon_{Hf}(t)$值[13]. 岩浆岩的全岩Hf和Nd表现出明显的相关性, 即$\varepsilon_{Hf}(t)=1.55\times\varepsilon_{Nd}(t)+1.21$, 而大洋沉积物则表现出显著的Hf和Nd同位素解耦, 即$\Delta\varepsilon_{Hf}(t)=\varepsilon_{Hf}(t)-1.55\times\varepsilon_{Nd}(t)-1.21$显著大于零[55]. 有大洋沉积物参与的弧岩浆岩会继承全岩Hf-Nd同位素解耦的特征.

硅同位素在浅地表生物作用过程中明显分馏. 海洋沉积物中的硅藻、海绵、放射虫等富硅生物优先吸取轻的硅同位素, 造成其具异常低的δ^{30}Si值(例如, 海绵δ^{30}Si为−6.74‰~−1.50‰). 对滇西大中河火山岩(420 Ma)研究发现其δ^{30}Si值极低(−0.47‰~−0.71‰), 说明只能继承于海洋沉积物, 与锆石Hf-O同位素模拟结果一致. 晚志留世原特提斯洋中富硅生物以海绵为主, 富硅生物海洋沉积物底辟与楔形地幔混合, 部分熔融形成低δ^{30}Si弧岩浆岩. 因此弧岩浆岩异常轻的硅同位素组成也是识别富硅大洋沉积物底辟到其源区的有力证据[13].

因元素Rb从海水中沉淀下来, 俯冲带沉积物往往具有低的Rb/Ba比值(小于0.1, 而蚀变洋壳Rb/Ba比值>0.35). 同时, 大洋沉积物的$\delta^{138/134}$Ba也相对较低(−0.2‰~+0.1‰), 源区有大洋沉积物物理混合的弧岩浆岩的$\delta^{138/134}$Ba也会明显降低[1,56]. 使用Rb/Ba和Ba同位素的二元图解可识别弧岩浆源区是否有大洋沉积物底辟体加入[1,17,56].

因此, 俯冲大洋沉积物底辟体与楔形地幔混合形成的弧岩浆岩具有低的δ^{30}Si和$\delta^{138/134}$Ba值、高$\varepsilon_{Hf}(t)$和δ^{18}O值、全岩Nd-Hf同位素解耦等特征.

3.3 如何识别源区是否有蚀变洋壳底辟体参与

蚀变洋壳分为高温和低温两类, 在俯冲带深部混入弧岩浆岩源区的主要为高温蚀变洋壳. 高温蚀变洋壳具有较地幔更轻的氧同位素值, δ^{18}O值远小于地幔值(5.3‰±0.3‰). 蚀变洋壳底辟体与楔形地幔混合产物的δ^{18}O会小于5.3‰±0.3‰. 俯冲带板片流体和熔体Mg^{2+}

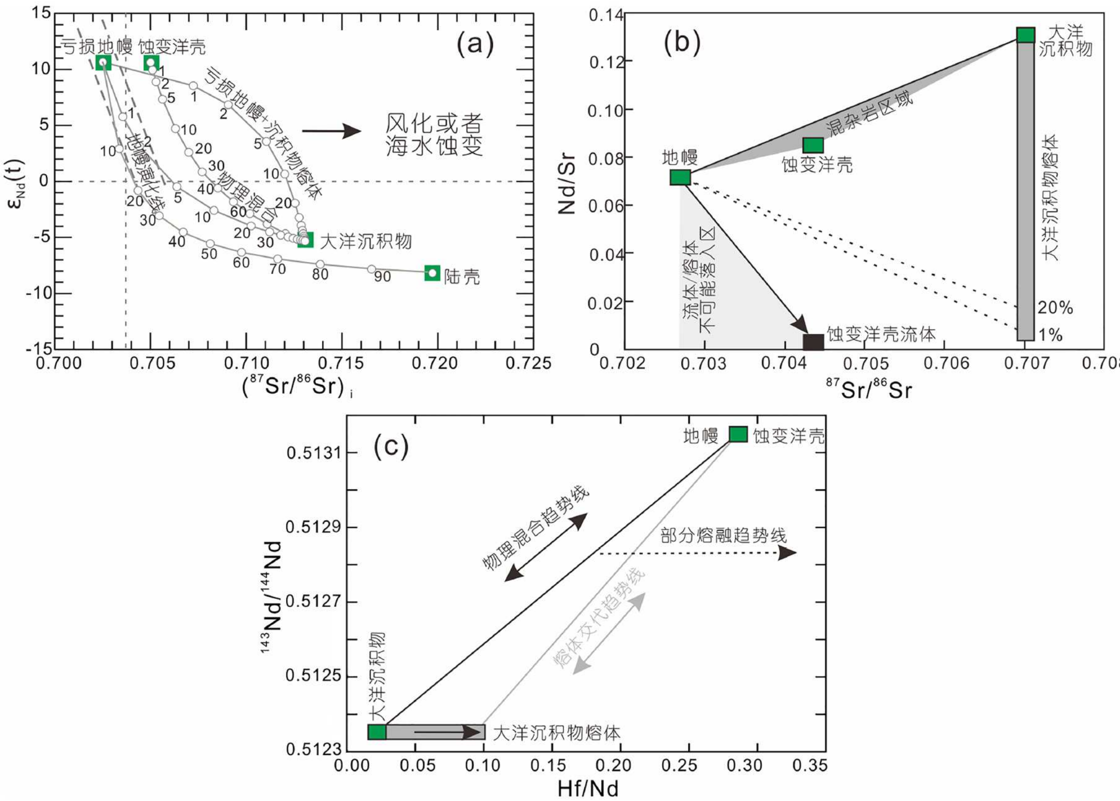

图 5 Nielsen和Marschall[14]建立的利用弧岩浆岩全岩Sr-Nd同位素和Sr-Nd-Hf微量元素比值来区分板片流体/熔体交代和板片混杂岩物理混合模式的图版. (a) Sr-Nd同位素二端元混合模拟结果. (b) Sr同位素与Nd/Sr比值的关系图. (c) Nd同位素与Hf/Nd比值图

Figure 5 Mixing diagrams established by Nielsen and Marschall[14] using the Sr-Nd isotope and Sr-Nd-Hf trace element ratios of arc magmatic rocks to distinguish between plate fluid/melt metasomatism and slab mélange physical mixing modes. (a) Sr-Nd isotope correlation and mixing modeling results. (b) Plots of Sr isotopes against Nd/Sr ratios. (c) Plots of Nd isotopes versus Hf/Nd ratios

富集Mg的轻同位素, 俯冲洋壳流体和熔体具低的Mg同位素值(低至−1.3‰), 而蚀变洋壳具有较高的δ^{26}Mg(分别高至0.15‰和0.10‰), 明显高于地幔橄榄岩(−0.26‰±0.02‰)[17]; Li是流体活动性元素, 板片脱水过程中重的Li同位素更倾向于进入流体中, 而残余蚀变洋壳具有轻的Li同位素组成. 因此, 受俯冲洋壳流体改造的地幔楔和板片混杂岩物理混合的地幔源区具有不同的Mg, Li同位素特征(前者低δ^{26}Mg、高δ^{7}Li; 后者高δ^{26}Mg、低δ^{7}Li). Liu等人[50]研究发现大兴安岭玛尼图(J_2mn)中-基性火山岩具高的δ^{26}Mg值(−0.15‰~+0.09‰), 高温蚀变洋壳底辟体与地幔混合才可形成如此高δ^{26}Mg值和Pb-Sr同位素比值. 同时该套火山岩具有非常低的δ^{7}Li值(−2.54‰~−1.31‰), 结合其Sr-Nd-Pb同位素组成, 说明其源区不是板片流体/熔体交代的地幔楔, 而是高温蚀变洋壳与地幔混合[50].

硼是一种流体活动性的可溶性元素, 其同位素在不同储库单元中分馏明显, 地幔中δ^{11}B为(−10‰~−7‰), 蚀变洋壳δ^{11}B为(0‰~+5‰), 沉积物δ^{11}B大部分小于0‰. 因此, 有高温蚀变洋壳参与的弧岩浆岩表现出相对重的B同位素值[45,57]. Zhang等人[58]通过对马里亚纳弧岩浆岩研究, 认为蚀变洋壳底辟形成的弧岩浆具有重的Ba同位素组成和Sr-Nd同位解耦的特征.

综上, 俯冲带板片混杂岩中蚀变洋壳底辟与地幔楔混合后熔融形成的弧岩浆具有重的Mg、B和Ba同位素组成, 以及低的O和Li同位素值.

4 板片混杂岩底辟体与弧下不同类型地幔相互作用的产物

俯冲带弧岩浆岩常被认为具有亏损高场强元素、富集大离子亲石元素的标志特征, 这类铌钽亏损弧岩浆岩根据其碱性元素含量可分为亚碱性和碱性两类. 此外, 在全球各地不同时代的俯冲带还有大量富集高场强元素的弧岩浆岩分布, 被称为富集铌钽弧岩浆岩[59~67]. 现有资料已证实上述三类弧岩浆岩(铌钽亏损

亚碱性弧岩浆岩、铌钽亏损碱性弧岩浆岩和铌钽富集弧岩浆岩)均可通过板片混杂岩底辟体与弧下地幔相互作用形成.

4.1 板片混杂岩与未被交代的弧下地幔混合可形成铌钽亏损亚碱性弧岩浆岩

铌钽亏损亚碱性弧岩浆岩是最常见的弧岩浆岩，其成因长期被地质学家解释为俯冲大洋板片流体/熔体交代的楔形地幔部分熔融而成. Codillo等人[11,68]使用板片混杂岩和亏损MORB(洋中脊玄武岩)型地幔橄榄岩的混合物在1.5 GPa和1150~1350°C的条件下开展了部分熔融实验，熔融产物为拉斑质至钙碱性的弧岩浆岩. 近年多个弧岩浆岩实例证实板片混杂岩与未被交代的弧下地幔混合可形成铌钽亏损亚碱性弧岩浆岩. 如Nielsen和Marschall[14]、Wu等人[1]、Maunder等人[69]和Zhang等人[58]分析了汤加、马里亚纳和小安的列斯群岛的弧岩浆岩元素和同位素地球化学特征，发现它们是板片混杂岩底辟体与弧下地幔物理混合的产物. Yan等人[46]对西藏林子宗亚碱性安山质弧火山岩的研究发现其成因与混杂岩底辟体部分熔融相关. 秦岭造山带的浮水早古生代基性弧岩浆岩也来源于弧下地幔与混杂岩底辟体物理混合物的部分熔融[17]. 中亚造山带南阿尔泰地区南天山变质杂岩中广泛分布的晚石炭世弧岩浆岩与弧下大规模的混杂岩底辟体相关[51]. Liu等人[54]对滇西大中河地区早古生代(420 Ma)亚碱性火山岩的研究发现其具有异常高的锆石δ^{18}O和异常低的δ^{30}Si值，这些特征只能继承于富硅的大洋沉积物底辟体. 以上资料表明板片混杂岩与未被交代的弧下地幔混合可形成铌钽亏损亚碱性弧岩浆岩.

4.2 板片混杂岩与低比例OIB(洋岛玄武岩)型地幔混合可形成铌钽亏损碱性弧岩浆岩

碱性中-基性岩浆岩的成因复杂，前人将其源岩归纳为三类：循环的洋壳[70]、陆下岩石圈地幔[71]和上涌OIB型软流圈地幔[72]. 洋壳具有低放射性Sr和高放射性Pb, Nd和Hf同位素, 其部分熔融产物将继承这些同位素组成，即低(^{87}Sr/^{86}Sr)i比值、高$\varepsilon_{Nd}(t)$和$\varepsilon_{Hf}(t)$值以及高(^{206}Pb/^{204}Pb)i、(^{207}Pb/^{204}Pf)i和(^{208}Pb/^{204}Pb)i比值. 洋壳的部分熔融将产生高Sr含量和高Sr/Y比值的埃达克岩浆. 陆下岩石圈地幔与正常地幔具有相似的O和Mg同位素，即δ^{18}O=+5.3‰±0.3‰, δ^{26}Mg=+0.26‰±0.02‰, 其部分熔融产物的δ^{18}O和δ^{26}Mg保持不变. 上涌的OIB型地幔岩浆具有EMI型地球化学特征，如夏威夷海岛玄武岩和峨眉山高钛玄武岩.

Liu等人[50]在研究大兴安岭中侏罗世玛尼图组碱性火山岩时，发现其与典型的OIB相比，微量元素蜘蛛图上Nb-Ta明显负异常. 这一特征在排除了大陆地壳混染和俯冲熔体/流体交代的可能性之后，只可能继承于上述三类源岩. 这类铌钽亏损碱性弧岩浆岩低Sr含量和低Sr/Y比值, 不具有埃达克岩特征, 无法直接由洋壳部分熔融形成. 其δ^{18}O值(+3.56‰~+5.12‰)显著低于地幔，δ^{26}Mg值(−0.168‰~0.009‰)又明显高于岩石圈地幔，因此玛尼图组碱性火山岩也不可能来源于岩石圈地幔部分熔融. 因此，玛尼图组碱性火山岩只能来源于上涌的OIB型地幔岩浆. 此外，其Sr-Nd-Pb同位素组成还说明俯冲板片混杂岩参与其成岩过程, 而O-Mg-Li同位素进一步确定其源区发生了高温蚀变洋壳底辟与OIB型地幔物理混合过程. 两端元物理混合模拟显示高温蚀变洋壳和OIB型地幔混合可形成玛尼图组碱性火山岩.

除此之外, Cruz-Uribe等人[15]开展的天然板片混杂岩在上地幔温压条件下部分熔融实验，证实可产生碱性岩浆岩. Ma等人[45]通过B同位素示踪发现青藏高原北部晚始新世富钾岩浆源区有混杂岩底辟体参与. Schaarschmidt等人[44]研究希腊东北部到土耳其西北部的渐新世爱琴海碱性弧岩浆岩后，提出大洋沉积物底辟体与弧下地幔混合之后低比例部分熔融可形成钾玄质弧岩浆. Wang等人[19]在研究西天山两套碱性弧岩浆岩时，发现区域内板片混杂岩在2.8~2.4 GPa和1.8~1.4 GPa及1000~1200°C的温度条件下部分熔融可形成与两套碱性弧岩浆岩相似的元素地球化学特征.

上述研究说明板片混杂岩与OIB型地幔混合可形成铌钽亏损碱性弧岩浆岩. 典型的OIB型地幔的铌钽元素在微量元素蛛网图上显著正异常，如在弧岩浆岩源区混入的OIB型地幔比例过高, 其产物铌钽亏损则不明显，甚至会正异常. 因此, 铌钽亏损碱性弧岩浆岩源区中OIB型地幔比例不会太高.

4.3 板片混杂岩与高比例OIB型地幔混合可形成铌钽富集弧岩浆岩

铌钽富集弧岩浆岩指具有TiO_2=1 wt.%~2 wt.%, Nb>7 ppm, 低LILE/HFSE和HREE/HFSE比值、蛛网图显示铌钽正异常或弱负异常等特征的基性岩浆岩[73~77]，当Nb含量大于20 ppm时也被称为高铌基性

岩[77,78]. 前人发现的绝大多数铌钽富集弧岩浆岩基本都与埃达克岩伴生, 所以铌钽富集弧岩浆岩常被认为起源于埃达克质熔体交代的楔形地幔. 但是埃达克岩和地幔楔橄榄岩都亏损铌钽[62,79,80], 二者相互反应如何富集铌钽一直难以解释清楚. 此外, 前人还提出地壳混染和俯冲洋壳部分熔融等铌钽富集弧岩浆岩成因模式, 但是地壳和俯冲洋壳部分熔融的产物(即埃达克岩)都是铌钽亏损的, 这两种成因同样也无法有效解释铌钽为何富集. 与常见的亏损铌钽岛弧岩浆岩相比, 铌钽富集弧岩浆岩成因研究的关键在于科学解释铌钽为何富集, 解释铌钽富集的关键在于找到铌钽富集的源区.

地幔端元中, OIB型地幔显著富集铌钽, 是一个潜在的富铌基性岩源区. 笔者在哀牢山构造带内发现白垩纪铌钽富集弧岩浆与OIB型基性岩伴生, 而哀牢山构造带甚至整个三江地区少见白垩纪埃达克岩报道. 哀牢山构造带白垩纪铌钽富集弧岩浆的稀土元素配分图和蛛网图较OIB要平缓很多, 说明还应该有另外一种地幔端元也参与了其形成过程. 两端元混合模拟发现15%的OIB型与85%岛弧型富集端元混合再部分熔融就可以很好解释哀牢山白垩纪富铌基性岩的形成过程[54,67]. 开展Sr-Nd-Pb-Mg-Li-Si-O同位素研究识别出其源区的岛弧型富集端元应为俯冲大洋板片混杂岩. 为了进一步验证这一成因机制, 笔者还发现了与OIB伴生的哀牢山志留纪富铌基性岩[66]、东北额尔古纳地块早白垩世富铌中基性火山岩[81]等. 对它们开展的元素和同位素联合示踪, 进一步证明了OIB型地幔与俯冲板片混杂岩混合然后部分熔融可形成富铌基性岩[54].

上述研究说明板片混杂岩与OIB型地幔混合可形成铌钽亏损碱性弧岩浆岩(图6). 典型的OIB型地幔铌钽元素在微量元素蛛网图上显示正异常或弱负异常, 如在弧岩浆岩源区混入的OIB型地幔比例过低, 则其产物的铌钽将会出现亏损. 因此, 铌钽富集弧岩浆岩源区中OIB型地幔比例不会太低.

5 现有认识、存在问题和未来研究展望

板片混杂岩底辟体与弧下地幔物理混合形成弧岩浆岩的过程在俯冲带真实存在, 其底辟过程可细分为大洋沉积物底辟、混杂岩(大洋沉积物和蚀变洋壳混合)底辟和蚀变洋壳底辟等三种方式. 多元同位素组成与微量元素比值的综合联用可区分板片流体/熔体交代和板片混杂岩物理混合两种模式. Sr-Nd-Pb等放射性同位素和O-Si-Mg-Ba-B等稳定同位素的联合示踪可进一步实现对弧岩浆岩源区是大洋沉积物底辟体还是蚀变洋壳底辟体的识别. 板片混杂岩与未被交代的弧下地幔混合可形成铌钽亏损亚碱性弧岩浆岩, 与低比例OIB型地幔混合可形成铌钽亏损碱性弧岩浆岩, 而与高比例OIB型地幔混合可形成铌钽富集弧岩浆岩.

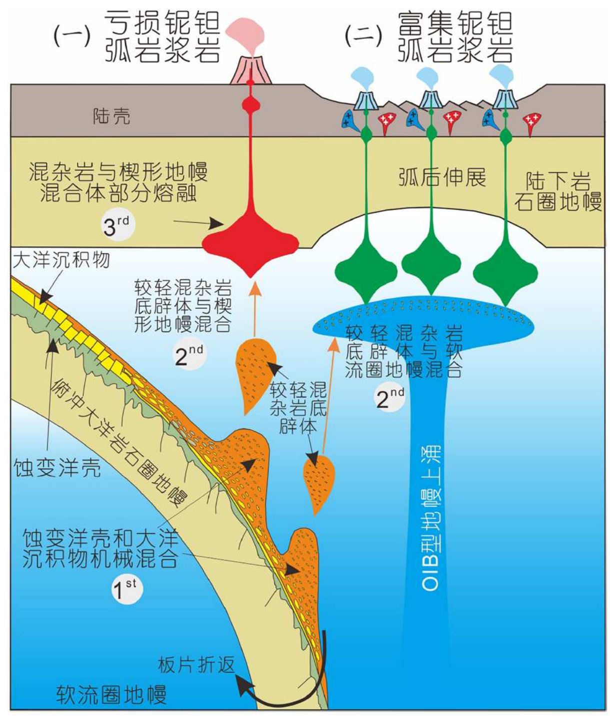

图 6 混杂岩底辟体与楔形地幔和上涌软流圈地幔物理混合的模式图

Figure 6 Schematic cartoon of subducted mélange recycling in upwelling OIB-like asthenosphere depicting two different trajectories for the buoyant mélange diapirs

近年板片混杂岩底辟体模型为解释俯冲板片混杂岩与弧下地幔相互作用过程提供了全新的思路, 前人也取得很多的认识和结论, 但板片混杂岩底辟的研究仍有一些问题亟待解决. (1) 混杂岩底辟过程中减压熔融广泛发生, 残留出露到地表的板片混杂底辟体鲜有报道, 因此目前仍缺少板片混杂底辟体存在的直接证据. 现在被报道的唯一可能的出露到地表的混杂岩底辟体是吉尔吉斯斯坦的Atbashi杂岩体, Sang等人[51]认为其中被包裹在变沉积岩中的高压/超高压变质岩是未熔融的混杂岩底辟体. 全球的俯冲带和造山带是否出露其他的混杂岩底辟体值得深入研究. (2) 针对俯冲带混杂岩底辟的过程和规模的认识值得深化. 当前就板片混杂岩底辟过程的认识主要依据数值模拟的手段, 但囿于模拟计算的局限性, 洋壳俯冲过程中多种矿物

相变和地幔水化如何影响混杂岩底辟仍是未知数. 混杂岩底辟过程和规模也需要深地震反射资料的精细刻画. (3) 板片混杂岩底辟和流体/熔体交代过程在同一俯冲带分别扮演什么角色, 二者是否共存, 也值得深入研究. 这些关乎精细认识壳幔相互作用过程的科学问题, 静待地质学家深入研究.

致谢 评审专家对本文提出的建设性修改意见, 使本文质量得以提高, 在此致以衷心的感谢!

参考文献

1 Wu F, Turner S, Schaefer B F. Mélange versus fluid and melt enrichment of subarc mantle: a novel test using barium isotopes in the Tonga-Kermadec arc. Geology, 2020, 48: 1053–1057
2 Zhu R, Zhao P, Wan B, et al. Geodynamics of the one-way subduction of the Neo-Tethys Ocean (in Chinese). Chin Sci Bull, 2023, 68: 1699–1708 [朱日祥, 赵盼, 万博, 等. 新特提斯单向俯冲的动力学机制. 科学通报, 2023, 68: 1699–1708]
3 Liao J, Qing J R, Wu Y M, et al. Dynamics of mid-ocean ridge-involved subduction (in Chinese). Chin Sci Bull, 2024, 69: 2534–2546 [廖杰, 卿佳容, 吴扬名, 等. 洋中脊俯冲的动力学过程. 科学通报, 2024, 69: 2534–2546]
4 Penniston-Dorland S C, Sorensen S S, Ash R D, et al. Lithium isotopes as a tracer of fluids in a subduction zone mélange: franciscan Complex, CA. Earth Planet Sci Lett, 2010, 292: 181–190
5 van den Boorn S H J M, van Bergen M J, Nijman W, et al. Dual role of seawater and hydrothermal fluids in Early Archean chert formation: evidence from silicon isotopes. Geology, 2007, 351: 939
6 Ishizuka O, Taylor R N, Milton J A, et al. Fluid–mantle interaction in an intra-oceanic arc: constraints from high-precision Pb isotopes. Earth Planet Sci Lett, 2003, 211: 221–236
7 Hasenclever J, Morgan J P, Hort M, et al. 2D and 3D numerical models on compositionally buoyant diapirs in the mantle wedge. Earth Planet Sci Lett, 2011, 311: 53–68
8 Gerya T V, Connolly J A D, Yuen D A, et al. Seismic implications of mantle wedge plumes. Phys Earth Planet Inter, 2006, 156: 59–74
9 Gerya T V, Yuen D A. Rayleigh–Taylor instabilities from hydration and melting propel ‘cold plumes’ at subduction zones. Earth Planet Sci Lett, 2003, 212: 47–62
10 Lin C H, Shih M H, Lai Y C. Mantle wedge diapirs detected by a dense seismic array in Northern Taiwan. Sci Rep, 2021, 11: 1561
11 Codillo E A, Le Roux V, Marschall H R. Arc-like magmas generated by mélange-peridotite interaction in the mantle wedge. Nat Commun, 2018, 9: 2864
12 Marschall H R, Schumacher J C. Arc magmas sourced from mélange diapirs in subduction zones. Nat Geosci, 2012, 5: 862–867
13 Liu H, Nielsen S G, Zhu G. Sponge-rich sediment recycling in a Paleozoic continental arc driven by mélange melting. Geology, 2023, 51: 75–79
14 Nielsen S G, Marschall H R. Geochemical evidence for mélange melting in global arcs. Sci Adv, 2017, 3: 1–7
15 Cruz-Uribe A M, Marschall H R, Gaetani G A, et al. Generation of alkaline magmas in subduction zones by partial melting of mélange diapirs—An experimental study. Geology, 2018, 46: 343–346
16 Little T A, Hacker B R, Gordon S M, et al. Diapiric exhumation of Earth’s youngest (UHP) eclogites in the gneiss domes of the D’Entrecasteaux Islands, Papua New Guinea. Tectonophysics, 2011, 510: 39–68
17 Hao L L, Nan X Y, Kerr A C, et al. Mg-Ba-Sr-Nd isotopic evidence for a mélange origin of early Paleozoic arc magmatism. Earth Planet Sci Lett, 2022, 577: 117263
18 Ho C Q. Conditions of Mélange Diapir Formation [B.S. thesis]: college Park, Maryland, University of Maryland, 2019. 1–28
19 Wang K, Cai K, Sun M, et al. Diapir melting of subducted mélange generating alkaline arc magmatism and its implications for material recycling at subduction zone settings. Geophys Res Lett, 2022, 49: e2021GL097693
20 Behn M D, Kelemen P B, Hirth G, et al. Diapirs as the source of the sediment signature in arc lavas. Nat Geosci, 2011, 4: 641–646
21 Mériaux C A, Duarte J C, Duarte S S, et al. Capture of the Canary mantle plume material by the Gibraltar arc mantle wedge during slab rollback. Geophys J Int, 2015, 201: 1717–1721
22 Tamura Y, Ishizuka O, Stern R J, et al. Two primary basalt magma types from northwest rota-1 volcano, mariana arc and its mantle diapir or mantle wedge plume. J Petrol, 2011, 52: 1143–1183
23 Castro A, Gerya T, Garcia-Casco A, et al. Melting relations of MORB-sediment melanges in underplated mantle wedge plumes; implications for the origin of cordilleran-type batholiths. J Petrol, 2010, 51: 1267–1295
24 Castro A, Gerya T V. Magmatic implications of mantle wedge plumes: experimental study. Lithos, 2008, 103: 138–148

25 Gorczyk W, Gerya T V, Connolly J A D, et al. Growth and mixing dynamics of mantle wedge plumes. Geology, 2007, 35: 587–590
26 Williams P R, Pigram C J, Dow D B, et al. Melange production and the importance of shale diapirism in accretionary terrains. Nature, 1984, 309: 145–146
27 Fei Q, Wang X P. A preliminary study on diapiric structure in oil and gas-bearing basins in Eastern China (in Chinese). Oil and Gas Geology, 1982, 3: 113–123 [费琪, 王燮培. 初论中国东部含油气盆地的底辟构造. 石油与天然气地质, 1982, 3: 113–123]
28 Becker D G, Cloos M. Melange diapirs into the cambria slab: a franciscan trench slope basin near Cambria, California. J Geol, 1985, 93: 101–110
29 Shreve R L, Cloos M. Dynamics of sediment subduction, melange formation, and prism accretion. J Geophys Res, 1986, 91: 10229–10245
30 Cowan D S. Structural styles in Mesozoic and Cenozoic mélanges in the western Cordillera of North America. Geol Soc Am Bull, 1985, 96: 451–462
31 Lash G G. Diverse melanges of an ancient subduction complex. Geology, 1987, 15: 652–655
32 Cloos M, Shreve R L. Subduction-channel model of prism accretion, melange formation, sediment subduction, and subduction erosion at convergent plate margins: 2. Implications and discussion. Pure Appl Geophys, 1988, 128: 501–545
33 Talbot C J, Brunn V. Melanges, intrusive and extrusive sediments, and hydraulic arcs. Geology, 1989, 17: 446–448
34 Raymond L A. Perspectives on the roles of melanges in subduction accretionary complexes: a review. Gondwana Res, 2019, 74: 68–89
35 Hall P S, Kincaid C. Diapiric flow at subduction zones: a recipe for rapid transport. Science, 2001, 292: 2472–2475
36 Zheng Y, Lay T, Flanagan M P, et al. Pervasive seismic wave reflectivity and metasomatism of the tonga mantle wedge. Science, 2007, 316: 855–859
37 Tamura Y, Tatsumi Y, Zhao D, et al. Hot fingers in the mantle wedge: new insights into magma genesis in subduction zones. Earth Planet Sci Lett, 2002, 197: 105–116
38 Zhao D, Hasegawa A, Kanamori H. Deep structure of Japan subduction zone as derived from local, regional, and teleseismic events. J Geophys Res, 1994, 99: 22313–22329
39 Zhang N, Behn M D, Parmentier E M, et al. Melt segregation and depletion during ascent of buoyant diapirs in subduction zones. JGR Solid Earth, 2020, 125: e2019JB018203
40 Klein B Z, Behn M D. On the evolution and fate of sediment diapirs in subduction zones. Geochem Geophys Geosyst, 2021, 22: e2021GC009873
41 Currie C A, Beaumont C, Huismans R S. The fate of subducted sediments: a case for backarc intrusion and underplating. Geology, 2007, 35: 1111–1114
42 Miller N C, Behn M D. Timescales for the growth of sediment diapirs in subduction zones. Geophys J Int, 2012, 190: 1361–1377
43 Hermann J, Rubatto D. Accessory phase control on the trace element signature of sediment melts in subduction zones. Chem Geol, 2009, 265: 512–526
44 Schaarschmidt A, Haase K M, Voudouris P C, et al. Migration of arc magmatism above mantle wedge diapirs with variable sediment contribution in the aegean. Geochem Geophys Geosyst, 2021, 22: 1–21
45 Ma L, Gou G N, Kerr A C, et al. B isotopes reveal Eocene melange melting in northern Xizang during continental subduction. Lithos, 2021, 392: 1–13
46 Yan H, Long X, Li J, et al. Arc andesitic rocks derived from partial melts of mélange diapir in subduction zones: evidence from whole-rock geochemistry and Sr-Nd-Mo isotopes of the paleogene linzizong volcanic succession in Southern Xizang. JGR Solid Earth, 2019, 124: 456–475
47 Xu J, Xia X P, Spencer C J, et al. Identification of High δ^{18}O adakite-like granites in SE Xizang: implication for diapiric relamination of subducted sediments. Geophys Res Lett, 2022, 49: 1–10
48 Gerya T V, Yuen D A. Robust characteristics method for modelling multiphase visco-elasto-plastic thermo-mechanical problems. Phys Earth Planet Inter, 2007, 163: 83–105
49 Gerya T V, Yuen D A. Characteristics-based marker-in-cell method with conservative finite-differences schemes for modeling geological flows with strongly variable transport properties. Phys Earth Planet Inter, 2003, 140: 293–318
50 Liu H, Huangfu P, Zhu G. High-temperature altered oceanic crust recycling into oceanic-island basalt−like mantle produces alkaline continental crust driven by mélange diapirs: insights from isotopic tracing and numerical modeling. Geol Soc Am Bull, 2023, 136: 1651–1660
51 Sang M, Tan Z, Xiao W, et al. Formation of the eclogites of the Atbashi complex, Kyrgyzstan, in a subduction zone mélange diapir. Commun Earth Environ, 2023, 4: 434
52 Li S, Wang Q, Zhu D, et al. Formation of continental crust by diapiric melting of recycled crustal materials in the mantle wedge. Geophys Res Lett, 2022, 49: e2021GL097515
53 Castro A, Rodriguez C, Fernández C, et al. Secular variations of magma source compositions in the North Patagonian batholith from the Jurassic to Tertiary: was mélange melting involved? Geosphere, 2021, 17: 766–785
54 Liu H, Hastie A R, Petrone C M. High-field-strength-element enriched arc rocks witness subducted mélange recycling in upwelling asthenosphere. Lithos, 2024, 464-465: 107411

55 Vervoort J D, Plank T, Prytulak J. The Hf–Nd isotopic composition of marine sediments. Geochim Cosmochim Acta, 2011, 75: 5903–5926
56 Nielsen S G, Shu Y, Auro M, et al. Barium isotope systematics of subduction zones. Geochim Cosmochim Acta, 2020, 275: 1–18
57 Zhang Y, Gaetani G, Zeng Z, et al. Halogen (F, Cl) concentrations and Sr-Nd-Pb-B isotopes of the basaltic andesites from the Southern Okinawa trough: implications for the recycling of subducted serpentinites. JGR Solid Earth, 2021, 126: e2021JB021709
58 Zhang Y X, Shu Y C, Turner S, et al. Deciphering contribution of recycled altered oceanic crust to Arc magmas using Ba-Sr-Nd isotopes. J Geophys Res-Sol Ea, 2024, 129: 1–13
59 Zhang T Y, Deng J, Wang M, et al. Geochemistry and genesis of the Nadun Nb-enriched arc basalt in the Duolong mineral district, western Xizang: indication of ridge subduction. Geosci Front, 2022, 13: 101283
60 Cai K, Sun M, Xiao W, et al. Petrogenesis of late Paleozoic tholeiitic, Nb-enriched, calc-alkaline and adakitic rocks in southwestern Mongolia: implications for intra-oceanic arc evolution. Lithos, 2014, 202-203: 413–428
61 Kerrich R, Manikyamba C, Williamson M C. Contemporaneous eruption of Nb-enriched basalts – K-adakites – Na-adakites from the 2.7 Ga Penakacherla terrane: implications for subduction zone processes and crustal growth in the eastern Dharwar craton, India. Can J Earth Sci, 2012, 49: 615–636
62 Castillo P R. Origin of Nb-enriched basalts and adakites in Baja California, Mexico, revisited: reply. Geol Soc Am Bull, 2009, 121: 1470–1472
63 Hollings P. Archean Nb-enriched basalts in the northern Superior Province. Lithos, 2002, 64: 1–14
64 Castillo P R. The origin of some of the adakite-like and Nb-enriched lavas in southern Philippines. Acta Petrol Sin, 2002, 18: 143–151
65 Wyman D A, Ayer J A, Devaney J R. Niobium-enriched basalts from the Wabigoon subprovince, Canada: evidence for adakitic metasomatism above an Archean subduction zone. Earth Planet Sci Lett, 2000, 179: 21–30
66 Liu H, Xia X, Lai C K, et al. Break-away of South China from Gondwana: insights from the Silurian high-Nb basalts and associated magmatic rocks in the Diancangshan-Ailaoshan fold belt (SW China). Lithos, 2018, 318-319: 194–208
67 Liu H, Wang Y, Cawood P A, et al. Episodic slab rollback and back-arc extension in the Yunnan-Burma region: insights from Cretaceous Nb-enriched and oceanic-island basalt–like mafic rocks. Geol Soc Am Bull, 2017, 129: 698–714
68 Codillo E A, Le Roux V, Klein B, et al. The ascent of subduction zone mélanges: experimental constraints on mélange rock densities and solidus temperatures. Earth Planet Sci Lett, 2023, 621: 118398
69 Maunder B L, Kendrick M A, Ribeiro J M, et al. A negligible role for forearc serpentinites and mélange diapirism in contributing halogens to Mariana arc magmas. Earth Planet Sci Lett, 2024, 625: 118498
70 Hofmann A W. Mantle geochemistry: the message from oceanic volcanism. Nature, 1997, 385: 219–229
71 Pilet S, Baker M B, Stolper E M. Metasomatized lithosphere and the origin of Alkaline Lavas. Science, 2008, 320: 916–919
72 Ruttor S, Nebel O, Nebel-Yacobsen Y, et al. Alkalinity of ocean island lavas decoupled from enriched source components: a case study from the EM1-PREMA Tasmantid mantle plume. Geochim Cosmochim Acta, 2021, 314: 140–158
73 Wang Q, Wyman D A, Xu J, et al. Triassic Nb-enriched basalts, magnesian andesites, and adakites of the Qiangtang terrane (Central Xizang): evidence for metasomatism by slab-derived melts in the mantle wedge. Contrib Miner Petrol, 2008, 155: 473–490
74 Castillo P R, Rigby S J, Solidum R U. Origin of high field strength element enrichment in volcanic arcs: geochemical evidence from the Sulu Arc, southern Philippines. Lithos, 2007, 97: 271–288
75 Castillo P R, Solidum R U, Punongbayan R S. Origin of high field strength element enrichment in the Sulu Arc, southern Philippines, revisited. Geology, 2002, 30: 707–710
76 Sajona F G, Maury R C, Bellon H, et al. Initiation of subduction and the generation of slab melts in western and eastern Mindanao, Philippines. Geology, 1993, 21: 1007–1010
77 Reagan M K, Gill J B. Coexisting calcalkaline and high-niobium basalts from Turrialba Volcano, Costa Rica: implications for residual titanates in arc magma sources. J Geophys Res, 1989, 94: 4619–4633
78 Castillo P R. Origin of the adakite-high-Nb basalt association and its implications for postsubduction magmatism in Baja California, Mexico. Geol Soc Am Bull, 2008, 120: 451–462
79 Wang Q, McDermott F, Xu J, et al. Cenozoic K-rich adakitic volcanic rocks in the Hohxil area, northern Xizang: lower-crustal melting in an intracontinental setting. Geology, 2005, 33: 465–468
80 Aguillón-Robles A, Calmus T, Benoit M, et al. Late Miocene adakites and Nb-enriched basalts from Vizcaino Peninsula, Mexico: indicators of East Pacific Rise subduction below southern Baja California? Geology, 2001, 29: 531
81 Liu H, Li Y, Wu L, et al. Geochemistry of high-Nb basalt-andesite in the Erguna Massif (NE China) and implications for the early Cretaceous back-arc extension. Geol J, 2019, 54: 291–307

Summary for “俯冲带板片混杂岩底辟作用”

Mélange diapirs in the subduction factory

Huichuan Liu[1,2], Yuejun Wang[3*] & Pengpeng Huangfu[4*]

[1] *State Key Laboratory of Petroleum Resources and Engineering, China University of Petroleum (Beijing), Beijing 102249, China*
[2] *College of Geosciences, China University of Petroleum (Beijing), Beijing 102249, China*
[3] *Guangdong Provincial Key Lab of Geodynamics and Geohazards, School of Earth Sciences and Engineering, Sun Yat-sen University, and Southern Marine Science and Engineering Guangdong Laboratory (Zhuhai), Zhuhai 519082, China*
[4] *State Key Laboratory of Earth System Numerical Modeling and Application, College of Earth and Planetary Sciences, University of Chinese Academy of Sciences, Beijing 101408, China*
* Corresponding authors, E-mail: wangyuejun@mail.sysu.edu.cn; huangfu@ucas.ac.cn

Subducted oceanic crust (i.e., subducted mélange) comprises marine sediments, altered oceanic crust (AOC) and mantle peridotite. Much debate exists concerning how the subducted oceanic crust interacted with the overlying mantle in subduction zones. Current debates focus on two principal interaction mechanisms between the subducted mélange and the sub-arc mantle: marine sediment melt and/or AOC fluid metasomatism on sub-arc mantle, and physical mixing of subducted mélange with sub-arc mantle. While the traditional metasomatic model (incorporating sediment melting with AOC/serpentinite dehydration) has dominated arc formation theories, recent thermal constraints challenge this paradigm. Sediment melting requires temperatures exceeding 1050°C at subduction zone pressures (2.7−5 GPa), conditions rarely attained along typical slab-mantle interfaces. Such high temperatures cannot be reached at similar pressures along the slab interface with the sub-arc mantle. Consequently, the mélange mixing model has gained increasing attention, proposing initial bulk mixing of marine sediments and AOC with mantle wedge material prior to subsequent melting/dehydration processes. Numerical simulations, seismic observations, and geochemical data confirm the viability of mélange diapirism as an alternative mechanism, though critical questions remain regarding: (1) interaction dynamics between slab-derived diapirs and mantle materials, (2) diagnostic geochemical signatures of mixing products, and (3) robust identification criteria for these processes. This article summarizes the previous researches on the mélange diapirs in recent years, and lists the evidences of the physical mixing between the mélange diapirs and sub-arc mantle.

Numerical simulation results reveal three evolutionary stages of mélange diapirism: (1) sediment-dominated, (2) sediment-AOC hybrid, and (3) AOC-dominated phases. Our synthesis of recent advances found that distinct isotopic fingerprints enable discrimination between metasomatic and physical mixing processes in arc magmatism. Sediment-rich diapirs exhibit low δ^{30}Si and $\delta^{138/134}$Ba values, coupled with elevated $\varepsilon_{Hf}(t)$ and δ^{18}O, alongside Nd-Hf isotopic decoupling. Conversely, AOC-dominated diapirs display heavy δ^{26}Mg and δ^{11}B with light δ^{7}Li and δ^{18}O signatures. Mantle hybridization experiments demonstrate: (1) mélange mixing with depleted MORB-type mantle generates Nb-Ta-depleted subalkaline magmas, (2) interaction with low-proportion OIB-type mantle produces alkaline arc magmas, while (3) high-proportion OIB mantle blending yields Nb-Ta-enriched compositions.

Three key challenges persist in mélange diapir research. (1) During mélange diapir upwelling, extensive decompression melting occurs, yet there are few documented cases of exposed mélange diapirs at the earth surface. This lack of tangible examples leaves a critical gap in direct evidence for their existence. It is also worth further studying whether mélange diapirs are preserved and exposed in global subduction zones and orogenic belts. (2) Current knowledge of mélange diapir dynamics in subduction zones relies heavily on numerical simulations. Due to computational limitations, key uncertainties remain regarding the effects of mineral phase transitions and mantle hydration during oceanic crust subduction. High-resolution deep seismic reflection data could provide essential constraints on the detailed processes and scales of mélange diapir formation and evolution. (3) The relative contributions of mélange diapirs versus fluid/melt metasomatism in subduction zones remain poorly understood. Further research is needed to clarify whether these processes operate independently or coexist, and how they collectively influence subduction zone dynamics.

slab mélange, diapirism, altered oceanic crust, sub-arc mantle, arc magmatic rocks

doi: 10.1360/TB-2025-0017